Graph-Search and Differential Equations for Time-Optimal Vessel Route Planning in Dynamic Ocean Waves

Gianandrea Mannarini, Deepak N. Subramani, Pierre F. J. Lermusiaux, *Member, IEEE*, and Nadia Pinardi

Abstract—Time-optimal paths are evaluated by VISIR ("discoVerIng Safe and effIcient Routes"), a graph-search ship routing model, with respect to the solution of the fundamental differential equations governing optimal paths in a dynamic wind-wave environment. The evaluation exercise makes use of identical setups: topological constraints, dynamic wave environmental conditions, and vessel-ocean parametrizations, while advection by external currents is not considered. The emphasis is on predicting the time-optimal ship headings and Speeds Through Water constrained by dynamic ocean wave fields. VISIR upgrades regarding angular resolution, time-interpolation, and static navigational safety constraints are introduced. The deviations of the graph-search results relative to the solution of the exact differential equations in both the path duration and length are assessed. They are found to be of the order of the discretization errors, with VISIR's solution converging to that of the differential equation for sufficient resolution.

Index Terms—Graph-search, time-optimal differential optimization, level set equations, reachability, ocean modelling, computational performance, VISIR.

I. INTRODUCTION

PATH planning problems are typically addressed by merging optimization algorithms with a modelling of the environment and the vehicle's interaction with it. The approximations and numerical errors of the algorithms used for path computation have rarely been documented or investigated. This may be due to the exact solution not being available, particularly for strong and dynamic environments. However,

the assessment of such errors is critical for real-world applications, including the optimization of road travel [1], the control of autonomous robots and vehicles in harsh or remote environments such as those that are chemically hazardous [2], in the open and deep ocean [3], in extra-terrestrial environments [4], climate-optimized aircraft routing [5], and ship routing [6]. Comparing the approximate approaches to exact solutions in optimal path planning is therefore of benefit. In addition to saving time and energy, truly optimal paths reduce the negative effects of transportation on the environment and their contribution to anthropogenic climate change [7].

In this study, we focus on the prediction of time-optimal paths for marine surface vessels sailing from one location to another, under the influence of a dynamic surface ocean gravity wave field that constrains the surface vessel motion. This is a common issue for ship operators. Speed loss in waves is due the degrees of freedom of the vessel and depends on the hull geometry, cf. Appendix A. Due to this effect, and also for safety reasons, waves eventually lead to an increase in travel time and energy usage of the vessel.

Several approaches have been developed for path planning in dynamic environments, which can also be considered for marine voyages. In one category of approach the optimal control problem is formulated on a graph and dynamic programming methods (e.g., [8], [9]): heuristic search schemes such as A^* and the Rapidly-exploring Random Tree (RRT, e.g., [10], [11]), and nonlinear convex optimization (e.g., [12]–[15]), or evolutionary algorithms (e.g., [16], [17]) are employed to solve the optimal control problem. In another category, obstacle avoidance is emphasised and potential field methods [18] or Voronoi diagrams [19] are utilized to identify safe routes. Another category utilizes Fast Marching Methods (FMM, [20], [21]) or wave front expansions ([**?**], [22], [23]). Fundamental differential equations governing the reachability front and time- and energy-optimal paths for vehicles navigating in strong, dynamic, and uncertain environments have recently been developed and used in real settings, e.g., [3], [24]–[29]. These differential equations provide the exact solution, so they are used here to evaluate the solution provided by a graph-search method.

Graph-search methods are powerful and commonly used in various R&D sectors [30]–[32]. However, using them to solve time-optimal path or shortest path problems (SPPs) in strong and dynamic environments presents challenges. Reference [33] first recognized that Dijkstra's approach can

be used (with suitable modifications to include dynamic edge weights) for finding time-dependent shortest paths. However, this approach implicitly assumes that waiting at nodes is possible before traversing each graph arc. The impact of allowing such waiting times was analysed in [34], and the authors noted that optimality of the modified Dijkstra's algorithm depends on the rate of change of arc weights, which determines the behaviour of the network. For the network to be of the First-In-First-Out (FIFO) type, this rate, if negative, should not exceed unity in magnitude (if the rate is positive the network is already FIFO). Notably, in such FIFO networks, the Bellman's principle of optimality holds. Therefore shortest paths exist, which are simple and concatenated, and can be computed by a modified Dijkstra's algorithm. However, in a non-FIFO network, the Bellman's principle of optimality no longer holds, and the shortest path may be not simple and concatenated, thereby preventing the nodes from being permanently labelled. The SPP then becomes computationally hard (e.g. super-polynomial [25]) and the paths computed by the direct use of the modified Dijkstra's algorithm are then sub-optimal. However, if a waiting time at the source node of the path is feasible, the modified Dijkstra's algorithm, which has the same complexity as that of the static version, can compute the optimal paths. Critically, this simplification only holds if there are no positive discontinuities of the arc weights as functions of time, which can be a major limitation. In a closely related work [35], attempts were made to establish the complexity for finding the optimum start time by considering a FIFO network (or a non-FIFO with waiting times at nodes). They proved that the computational cost of their *arrival function* (i.e. start time plus travel time) is non-polynomial. Even a variational approach to SPP, as noted by [36], fails to find a global optimum in the presence of obstacles or a spatially non-convex cost. The author showed that a Hamilton-Jacobi (HJ) equation should be solved in such a case. He established an algorithm, which by mimicking that of Dijkstra, solves a numerical approximation of the HJ and predicted that methods for propagating wavefronts or level-sets could be even more appropriate. Finally, if flow advection by the dynamic environment is strong, i.e., its speed is greater than the vehicle speed, then local controllability issues will arise in graph-search methods, as pointed out in [25].

A. Other Methods

A* [10], [37] is an extension of Dijkstra's algorithm for least-distance paths. It differs from Dijkstra's in the fact that the search is biased towards the destination by using heuristics. It is still guaranteed to recover the optimal path (as Dijkstra does) if the heuristics satisfy an admissibility requirement. D* [38] generalizes A* to real-time planning in environments with dynamic obstacles, as it can update edge weights during the computation. Another difference of D* with respect to both A* and Dijkstra's algorithms is that it uses a backwards search from the goal node.

RRT [39] is a stochastic technique for effectively generating random points linked to a vertex and avoiding obstacles. Thus, RRT can be used for computing least-distance paths, while an efficient and accurate extension to least-time paths in a dynamic environment is not obvious.

Potential Field methods [18], [40] introduce a representation of obstacles through a function similar to an energy potential. The routing problem is then driven by repulsion from obstacles and attraction towards the goal location. The method introduces subjective parameters representing the obstacle and, depending on the energy landscape, may retrieve only suboptimal (locally optimal) paths.

Voronoi diagrams [19] have been utilized to identifying minimum distance paths in a partitioned domain.

FMM [20] solve the Eikonal equation to compute time-optimal paths and is inspired by and mimics Dijkstra's algorithm. FMM correspond to a special case of the governing HJ equation solved in the limiting case of local controllability, i.e. when currents are always weaker than the vehicle's speed (see Sect. II).

We are not aware of any applications of A*, D*, RRT, potential field, Voronoi diagrams, and FMM to least-time path planning in dynamic environments where the vehicle is under the influence of such strong advection (e.g. by dynamic winds or currents of speed greater than that of the vehicle).

B. VISIR and Its Evaluation

VISIR ("discoVerIng Safe and effIcient Routes") is a path planning model based on a time-dependent version of Dijkstra's algorithm, which is fully integrated with operational physical oceanography products [41], [42]. This has been validated with both static and time-dependent analytical benchmarks in [43]. However, the subtlety of the time-dependent SPP on graphs discussed above makes a more thorough evaluation necessary.

Thus, in the present manuscript the performance of VISIR is evaluated by comparing it to the exact governing time-optimal partial differential equation (PDE) [24]–[26]. This governing PDE contains three terms: a time-rate of change, a propulsion term with a vehicle speed accounting for speed loss in waves, and an advection term that governs current- and wind-induced transport [25].

However, in this initial comparison, VISIR can only compute optimal paths for surface vessels in the presence of waves [41]. Thus, the focus of this work is restricted to time-optimal route planning for vessels operating in dynamic ocean waves. The inclusion of waves into the PDE model requires the parametrization of speed loss in waves, which was taken from VISIR (cf. Appendix A) to allow for direct comparisons. Currents were only included in VISIR after the present work was completed, which is described in [43].

C. Outline of the Manuscript

We first briefly describe the VISIR planner and some of its specific components, and the differential time-optimal path planning in Sect. II. In our investigation, new technical features needed to be developed in VISIR, which are first introduced in Sect. III. The optimal paths and computational cost of the VISIR system are then compared to those of the governing differential equations for time-optimal path planning in dynamic environments and are provided in Sect. IV. Finally, conclusions are drawn in Sect. V.

II. OPTIMAL PATH PLANNING METHODS

The present problem consists of predicting the time-optimal path of a surface vessel sailing from one location to another within a dynamic ocean surface gravity wave field that constrains the vessel cruising speed. The waves can be provided either as analysis or forecast fields and the corresponding constraints on the ship motions are modelled and assumed known.

Problem Statement: Mathematically, the problem to be solved is to predict the path $\mathbf{x}^*(t) : [0, T^*] \rightarrow \Omega \subset \mathbb{R}^2$ of a vessel moving between an assigned start $\mathbf{x}(0) = \mathbf{x}_A$ and an end location $\mathbf{x}(T^*) = \mathbf{x}_B$ in a minimum time duration T^*, given that the vessel sails at a time-dependent flow-relative speed $F(\mathbf{x}, t)$, a.k.a. Speed Through Water (STW). $F(\mathbf{x}, t)$ includes the speed loss due to the dynamic inhomogeneous wave field.

In the present work, we evaluate the capacity of the graph-search method (VISIR) to solve the above minimization problem in a dynamic environment by comparing it with the numerical solution of the exact HJ equation for the signed distance or level-set-equation (LSE). These two methodologies are described in the following two subsections.

A. Graph-Search Method (VISIR)

The graph-search method is implemented in the VISIR model. It is distributed as free and open source software[1]. VISIR is the basis of an operational service for motorboat route planning in the Mediterranean Sea [42], which can also be used by sailboats [44].

Central to VISIR is the assumption of piecewise uniform motion, according to the trajectory differential equation

$$\frac{dx}{dt} - F(\mathbf{x}, t) = 0 \qquad (1)$$

that simply relates the time-rate of the change of vessel position to vessel STW. Here we refer to the VISIR version that allows for vessel speed variations in time and space but neglects the advection caused by environmental flows $\mathbf{V}(\mathbf{x}, t)$ (e.g. by ocean currents). This reflects the VISIR version at the time of this paper's submission, but it has since been extended to include also advection by ocean currents [43].

Paths of minimum travel time are obtained using vessel heading as the control variable. The inter-nodal connections of the graph (or "arcs") are assigned and they determine the angular resolution, cf. Sect. III-A. Arc weights dt are obtained from (1), which is discretized by approximating dx/dt with its finite difference quotient. This leads to a first order truncation error. Finally, a graph search method is run, where the arc weights are space and time-dependent quantities obtained from the discretization of (1). The graph search method used is a modified Dijkstra's algorithm [45] for dealing with time-dependent arc weights, cf. Sect. III-C. It returns, through the orientation of the arcs, an estimate of the optimal control policy, i.e., the optimal sequence of headings. In Sect. IV-B we show that, with sufficiently fine grid resolution, Dijkstra's algorithm converges to the exact solution, but only for FIFO

[1]www.visir-model.net

networks and if the motions are not affected by environmental flows larger than the nominal vehicle speed. In particular, for the present cases with zero ocean advection (1), the vessel heading is identical to the course over ground. Other technical features already implemented in VISIR include:

1) Shortest Path Algorithm Costs: For Dijkstra's algorithm with static arc weights, the computational cost for path computation scales as the square of the number n_g of grid points or, if a convenient data structure is used, as $n_g \log(n_g)$. The data structure will not reduce the number of graph nodes n_g expanded by the algorithm, but can facilitate operations on the list of nodes, such as insertion, removal, and minimum search [46] without improving the scaling of the worst-case estimate. While such data structures are not as yet used in VISIR, it does make use of a "forward star" representation [47]. This is a cleverer storage scheme used for maintaining and updating intermediate results. It has a beneficial effect on Djikstra's algorithm performance, without changing its worst-case estimate. In a forward star representation, the shortest path algorithm is provided with the list of all outgoing arcs from each graph node. Furthermore, a pointer is maintained with each node for speeding up access to its incidence list. This network representation improves the performance of the algorithm, as the full list of graph nodes is not accessed.

For the dynamic Dijkstra's algorithm, the computational cost depends on how often the arc weights are updated. More details on this can be found in Sect. III-C.

2) Coastal Navigation: VISIR was originally designed for short-sea shipping. Its capacity to deal with complex coastline and shoals is based on masking, cf. Sect. III-B. An option for controlling the minimum offshore distance can be used [42]. When the spatial resolution of the graph grid is higher than the wave forecast resolution [48], fields are extrapolated inshore through a "sea-over-land" procedure in the coastal zone [41]. Other extrapolations would also be possible, such as Laplace interpolation (e.g., [49], [50]) to diffuse data to the higher resolution grid points, which were previously land.

Synthetic information about how vessel interaction with waves is modelled is given in Appendix A. Other algorithmic updates of VISIR are reported in III and Appendix B.

B. Differential Path Planning (LSE)

For a ship moving from point A to point B in a strong and dynamic environment, the exact reachability front, i.e., the set of all points that can be reached by the vehicle in a given time, is governed by the HJ equation

$$\frac{\partial \phi(\mathbf{x}, t)}{\partial t} + F(\mathbf{x}, t)|\nabla \phi(\mathbf{x}, t)| + \mathbf{V}(\mathbf{x}, t) \cdot \nabla \phi(\mathbf{x}, t) = 0 \quad (2)$$

with initial conditions $\phi(\mathbf{x}, 0) = |\mathbf{x} - \mathbf{x}_A|$ and appropriate boundary conditions for coastlines and the open ocean [25]. Here, $\phi(\mathbf{x}, t)$ is a scalar reachability front tracking level set function (e.g., the signed distance field). The zero level set contour of the solution of (2) at $t > 0$ is the reachability front for a vehicle starting from $\mathbf{x}_A$ at $t = 0$, and the first time t at which the zero level set contour reaches the target B. The exact time-optimal path $\mathbf{X}^*(t)$ can be extracted from the time series

of zero level set contours by solving the particle backtracking ordinary differential equation (ODE)

$$\frac{d\mathbf{X}^*(t)}{dt} = -F(\mathbf{X}^*(t),t)\frac{\nabla\phi(\mathbf{X}^*(t),t)}{|\nabla\phi(\mathbf{X}^*(t),t)|}$$
$$- \mathbf{V}(\mathbf{X}^*(t),t),$$
$$\mathbf{X}^*(T^*(\mathbf{x}_B;\mathbf{x}_A)) = \mathbf{x}_B. \tag{3}$$

Thus, time-optimal path planning consists of two steps: *i)* the propagation of the reachability front by numerically computing the viscosity solution of (2); *ii)* computation of the time-optimal trajectory by solving (3) (to be understood in the generalized gradient sense).

Numerical schemes have been developed to complete the above steps [25] and generalized for various optimality criteria, including the time-, energy-, coordination-, and interception-optimal planning of swarms of AUVs in realistic data-assimilative dynamic ocean re-analyses [26], [51]–[56]. This was also recently utilized successfully in real-time exercises at sea with real AUVs [28], [57].

In the following we refer to the level-set-based numerical method used to solve the differential time-optimal path planning equations as the LSE method. It has several useful features and below we list those relevant to ship routing.

1) Exact Solution in Strong Advection and Dynamic Environments: The solution of the level-set PDEs, Eq. (2-3), is the exact time-optimal path between given endpoints, whenever such a path exists. This is true even in challenging situations, such as when multiple equivalent optimal paths exist or there are strong environmental fields. In fact, for both these situations the reachability front tracking level-set fields become non-differentiable. However, the viscosity solution of the HJ equation (2) has weak requirements in this field, namely to be Lipschitz-continuous.

When currents are stronger than a ship's speed, local controllability is an issue. This is accounted for by the LSE solution, e.g., [25]. Classic graph-based methods are, however, not guaranteed to provide the true solution in this case, hence we do not include currents in the present evaluation of VISIR.

Finally, as for other consistent and stable numerical solutions of PDEs [58], [59], the solution of (2) converges to the true solution as the spatial and temporal resolution is increased.

2) Computational Cost: The computational cost of solving the level-set advection PDE scales linearly with the number n_g of grid points [**?**], [24], [25]. In addition, to track the reachability front accurately, the PDE can be solved only in a narrow band of points around the zero level-set contour instead of the whole domain. This further reduces the computational effort required. The reachability fronts contain paths to all the reachable points for the vehicle, starting from A at time $t = 0$. Thus, if a different endpoint other than B or multiple end points anywhere in the domain are desired, only a scalar backtracking ODE needs to be solved for each end point, the computational cost of which is very cheap and also scales linearly with the number of path waypoints desired. The LSE cost linearity is inherent to the PDE solver [25], regardless of whether a narrow band is used or not. In the present study,

the LSE computation is completed over the whole domain (i.e. without a narrow band) to ensure that VISIR and LSE operate on the same number of grid points.

The total computational cost also scales linearly with the number of time steps. For the present application, this is chosen to satisfy a Courant-Friedrich-Levy (CFL) condition [25] for the problem with the highest mesh resolution, and then kept roughly constant, cf Tab. II. If a narrow-band spatial discretezation is used to evolve the zero level-set using only the necessary degrees of freedom (e.g. the necessary finite-volumes), the computational cost is further reduced [25].

Finally, we note that the LSE grid can be coarsened in space and/or in time to reduce the computational cost, just as the number of graph nodes can be reduced in the VISIR scheme. The accuracy of the solutions of both approaches will thus be reduced, as they are optimal for coarsened or averaged/smoothed dynamic wave field and coastlines. For balance, we use the same resolution for both LSE and VISIR when directly comparing their solutions.

3) Starting Time: In addition to computing the time-optimal path for a given start time, the level-set PDEs can also be used to determine the optimal vehicle start time and thus reach the desired end point in the quickest time. In the presence of adverse environmental conditions, this start time may be later than the earliest possible [25].

III. EVALUATION APPROACH AND UPDATES TO VISIR

To evaluate the solution computed by VISIR, we compare it with the time-optimal path computed by solving the LSE with speed loss in waves provided by the same vessel response parametrization of VISIR, but without current advection. The latter is a simplification when compared to previously published time-optimal planning for AUVs and gliders in which vehicles speeds were similar to those of currents. As there are no advection terms and the ship speed is always positive in our case, the ship can always get to the destination in a finite time. As the spatial and temporal resolution are increased, a graph-search scheme such as the modified Dijkstra's algorithm and a numerical solver for the level-set PDE are expected to provide solutions that converge with each other.

For this evaluation, the overall sequence of VISIR and LSE steps is summarized in Fig. 1. First, a $G(\nu, \Delta x)$ graph with order of connectivity ν and mesh resolution Δx is prepared, ensuring that the shoreline-crossing arcs are pruned. VISIR is then run on the $G'(\nu, \Delta x)$ graph resulting from this pruning. Subsequent steps include the computation of the vessel response function (Appendix A), a land-sea mask, and the regridding of the wave field on the grid of $G'(\nu, \Delta x)$. Both the vessel response function and the mask are used for the initialization of LSE. Thus, it is ensured that both VISIR and LSE use exactly the same bathymetry, shoreline, input forecast fields, and vessel response function. The evaluation is then restricted to the effect of the subsequent steps (those below the darker arrows in Fig. 1).

For VISIR, these are: a further pruning of $G'(\nu, \Delta x)$ accounting for Under Keel Clearance (UKC), resulting in a new graph, $G''(\nu, \Delta x)$; the computation of the arc weights dt defined by (1); and the run of the shortest path algorithm.
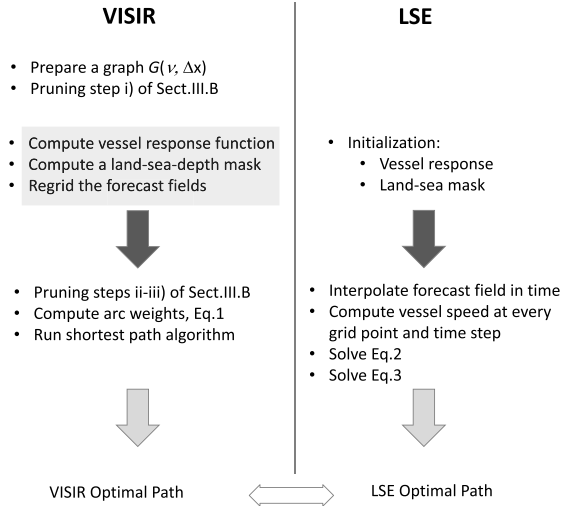
Fig. 1. Summary of main steps of the VISIR-LSE comparison strategy. The shaded box contains the VISIR steps and the outcome is used in the LSE runs. The steps below the darker arrows are the objects of the present evaluation exercise.

Fig. 2. Stencil of graphs $G(\nu = \{1, 4\}; \Delta x = \overline{OH_1})$ of variable path resolution $\overline{OP_\nu}$. The $\nu(\nu + 1)$ nodes within a single quadrant are displayed as filled circles (their pattern distinguishes between nodes linked to O at successive ν values). The minimum resolved angle is $\widehat{H_\nu OP_\nu}$. Other arcs of $G(\nu; \Delta x)$ are not displayed. Here, the path resolution $\Delta P = \overline{OP_\nu}$ varies with the graph order ν.

TABLE I
CONNECTIVITY AND RESOLUTION PARAMETERS FOR GRAPHS
WITH SQUARED MESHES

ν	$\mathcal{D}_\nu$	$\Delta\theta[^o]$	$\Delta P/(\sqrt{2}\Delta x)$	
			Eq.(6)	Eq.(7)
1	8	45.0	1.000	0.900
2	24	26.6	1.581	1.525
3	48	18.4	2.236	2.198
4	80	14.0	2.916	2.886
5	120	11.3	3.606	3.582
6	168	9.5	4.301	4.282
7	224	8.1	5.000	4.983
10	440	5.7	7.106	7.095
20	1680	2.9	14.160	14.154

For LSE, these are: the time-interpolation of the forecast field, the computation of the vehicle's speed at each grid point in space and time; and the solution of (2-3). Both VISIR and LSE optimal paths and kinematic quantities are then extracted and compared, as described below.

To increase the accuracy of VISIR, we conducted technical developments with respect to the previously published version [41]. These involved the graph order of connectivity, the masking procedure, and the use of a temporal interpolation for the edge weights. We present these in the following subsections and then use them in the actual evaluation and comparison experiments of Sect. IV.

A. Graph Order of Connectivity

To smooth the VISIR paths, an increase in its angular resolution is realized by additional graph edges. However, it is essential that this is accompanied by an increase in the horizontal resolution of the graph mesh. If not, new directions are created by the additional edges, but their lengths increase. This in turn reduces the accuracy of the representation of the environmental field (significant wave height and direction) on the graph, which is given by the average of its values at the graph nodes. The wave height field then determines the travel time along the edge, and thus contributes to the total duration of the voyage T^*, which is the objective of the optimization algorithm and the metrics used for validating VISIR vs. LSE.

VISIR graph nodes were previously linked only to all other nodes reached via either one or two hops. In this work, a larger number of hops is allowed. For a maximum of ν hops, in a directed graph with a squared mesh there are

$$\mathcal{D}_\nu = 4\nu(\nu + 1) \qquad (4)$$

such arcs (cf. Fig. 2). The number ν is the order of connectivity and $\mathcal{D}_\nu$ is the "average degree of the graph" [60].

While in [41] only $\nu = 2$ was used, in the present work graphs up to $\nu \leq 7$ were produced. This enables the angular
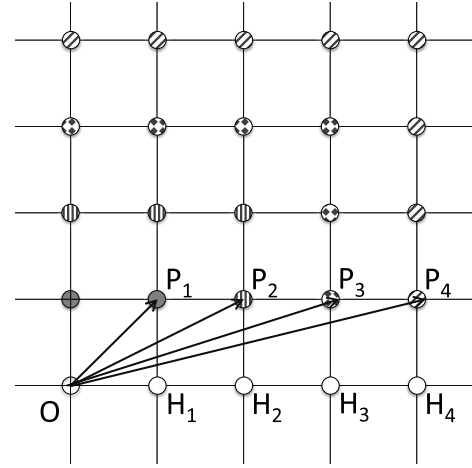
resolution $\Delta\theta$ (corresponding to angle $\widehat{H_\nu OP_\nu}$ of Fig. 2) to be increased up to:

$$\Delta\theta = \arctan(1/\nu) \qquad (5)$$

Values of $\Delta\theta$ and the number of outgoing arcs per node are reported for various ν in Tab. I.

Several authors using graph-search methods have built graphs with a higher ν for enhancing the smoothness of the paths, cf. [61], [62] and [63]. However, a point that has until now been disregarded (apart from a suggestion in the geometrical construction of [61]) is that acting on just the order of connectivity also alters the length of the arc realizing the finest angular resolution. This length is hereafter referred to as the path resolution ΔP, cf. Fig. 2.

The arc weights are computed by VISIR as an average of the field values at the nodes. As ΔP increases, the accuracy of the estimation of the arc weights, and particularly vessel speed, decreases. Thus, to increase the angular resolution without degrading the path resolution, it is necessary to refine the graph mesh spacing Δx. By requiring that the length of the arc leading to $\Delta\theta$ of (5) remains constant as the connectivity is increased, the following relation is derived:

$$\Delta P/\Delta x = \sqrt{1 + \nu^2} \qquad (6)$$

This article has been accepted for inclusion in a future issue of this journal. Content is final as presented, with the exception of pagination.

6

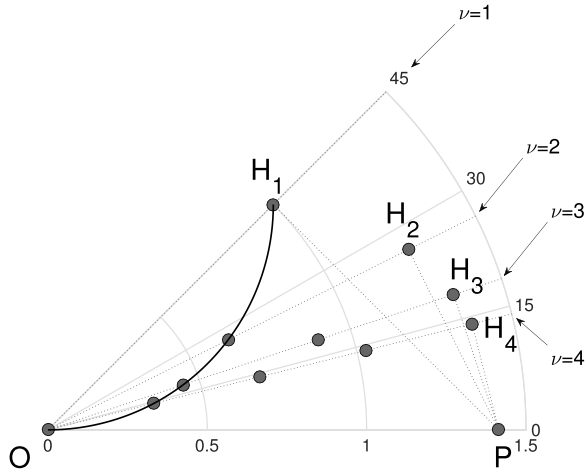IEEE TRANSACTIONS ON INTELLIGENT TRANSPORTATION SYSTEMS

Fig. 3. Stencil of graphs $G(\nu = \{1,4\}; \Delta x = \overline{OP}/\sqrt{1+\nu^2})$ of constant path resolution $\Delta P = \overline{OP}$. For a given ν, the gridpoints are aligned along the angle $\Delta\theta$ defined by (5) and their spacing $\Delta x/\overline{OH_1}$ as a function of $\Delta\theta$ is the solid line per O and H_1. Angles $\widehat{OH_\nu P} = 90^o$ $\forall \nu$ correspond upon axes tilting to $\widehat{OH_\nu P_\nu}$ of Fig. 2.

The graphical construction of Fig. 3 makes it clear that the path resolution is $\Delta P = \sqrt{2}\,\Delta x_1$ (with $\Delta x_1 = \overline{OH_1}$) for all graphs satisfying (6). The $\Delta P/(\Delta x\sqrt{2})$ ratio represents the refinement factor of the mesh spacing with respect to the $\nu = 1$ case, which is necessary to maintain a constant path resolution ΔP.

By computing the limit value of both (5) and (6) for $\nu \to \infty$ it is found that:

$$\Delta x = \Delta P \cdot \Delta\theta \tag{7}$$

(with $\Delta\theta$ in radians). That is, for preserving path resolution in graphs of a higher order of connection, mesh spacing Δx must increase proportionally to angular resolution $\Delta\theta$. In practice, as seen from the last two columns in Tab. I, the error committed using Δx from (7) with respect to (6) is already below 1% for $\nu \geq 5$.

B. Masking

To account for landmass and shallow waters, before the run of the shortest path algorithm in VISIR the graph is processed by removing ("pruning") some of its arcs:

i) Arcs intersecting the shoreline are all pruned;
ii) The depth of an arc is taken to be the minimum depth at either arc node. Unsafe arcs, i.e. arcs whose depth is smaller than the vessel draught (UKC≤0) are pruned.

This two-step processing corresponds to the masking procedure described in [41]. However, it can lead to a failure in some cases, and safe ν-hop arcs ($\nu \geq 1$) intersecting unsafe 1-hop arcs will not be pruned by step ii). To amend this, a third pruning step is applied in this work:

iii) If a ν-hop arc ($\nu \geq 1$) intersects with an unsafe 1-hop arc, and this intersection is not at the head or tail of either arc, the ν-hop arc is pruned.[2]

[2]Arc intersection may occur at various positions along the arc. E.g. in Fig. 2 $\overline{OP_2}$ (a 2-hop arc) intersects both $\overline{H_1\,P_1}$ and $\overline{H_2\,P_2}$ (both 1-hop arcs). While intersection with $\overline{H_2\,P_2}$ occurs at $\overline{OP_2}$'s head node (P_2), intersection with $\overline{H_1\,P_1}$ occurs at a point that is neither head nor tail of either arc

In Sect. IV-A we report a specific effect of step iii) for the case study considered.

In LSE, the equations are not simply solved under the mask, and island boundary conditions are utilized [51]. Therefore, no special pruning or treatment is necessary in the set-up of the reachability analysis.

C. Temporal Interpolation

Operationally, the wave forecasting is completed before the ship routing computations. Thus, the wave forecasts are only available at output times, Δ_{tE} of the wave model, whereas the path planner usually has a finer temporal resolution Δ_t. Therefore, a temporal interpolation scheme is used to estimate the environmental conditions at the temporal resolution of the planner. For LSE, this is simply a linear interpolation from Δ_{tE} to Δ_t. For VISIR, prior to the present comparison, arc weights were evaluated at the earliest possible time-step, ℓ[3],

$$\ell = 1 + \text{floor}(\tau_j/\Delta_{tE}) \tag{8}$$

with the time τ_j needed for reaching ("expanding") node j along the shortest path ($\tau_1 = 0$ at the start node 1) and the time-step duration Δ_{tE}. If τ_j does not coincide with the onset of a new time-step of the wave field, (8) still forces the evaluation of the arc weight at the time of the onset. The arc weights are thus kept constant during each time-step of the wave field. The advantage of this approach is a computational cost identical to that of a static algorithm [34]. The limit of this approach is the representation of rapidly varying environmental conditions. To improve this situation, the arc weights are evaluated at the exact time the tail node is expanded. This is achieved by linear interpolation in time, i.e., the real number $\mathcal{L}$ is computed:

$$\mathcal{L} = 1 + \tau_j/\Delta_{tE} \tag{9}$$

and a linear interpolation in time of the arc weight is performed to estimate their value at $t = \mathcal{L}$. The related logical modifications to the pseudocode of the VISIR shortest path function are reported in Appendix B.

IV. RESULTS

To assess the impact of the evaluation strategy and the advances of VISIR described in Sect. III, we focus on the case study #1 of [41]. This is a path planning exercise for a ferryboat crossing the Sicily Channel (about 120 nmi[4]) during a severe storm, with waves up to more than 5 m in terms of significant height. The sea state corresponds to analysis fields of an operational implementation of a NEMO-WW3 coupled model in the Mediterranean Sea [48]. The interaction between the ferryboat and the waves is based on a parametrization of wave-added resistance, as in Appendix A. An account of the circulation pattern in this part of the sea is given in [64].

The time-optimal route is then computed using (1) for preparing the arc weights and Dijkstra's method in VISIR and

[3]The function `floor` rounds to the nearest integer less than or equal to its argument.

[4]nmi = nautical mile = 1 852 m.

This article has been accepted for inclusion in a future issue of this journal. Content is final as presented, with the exception of pagination.

MANNARINI *et al.*: GRAPH-SEARCH AND DIFFERENTIAL EQUATIONS FOR TIME-OPTIMAL VESSEL ROUTE PLANNING
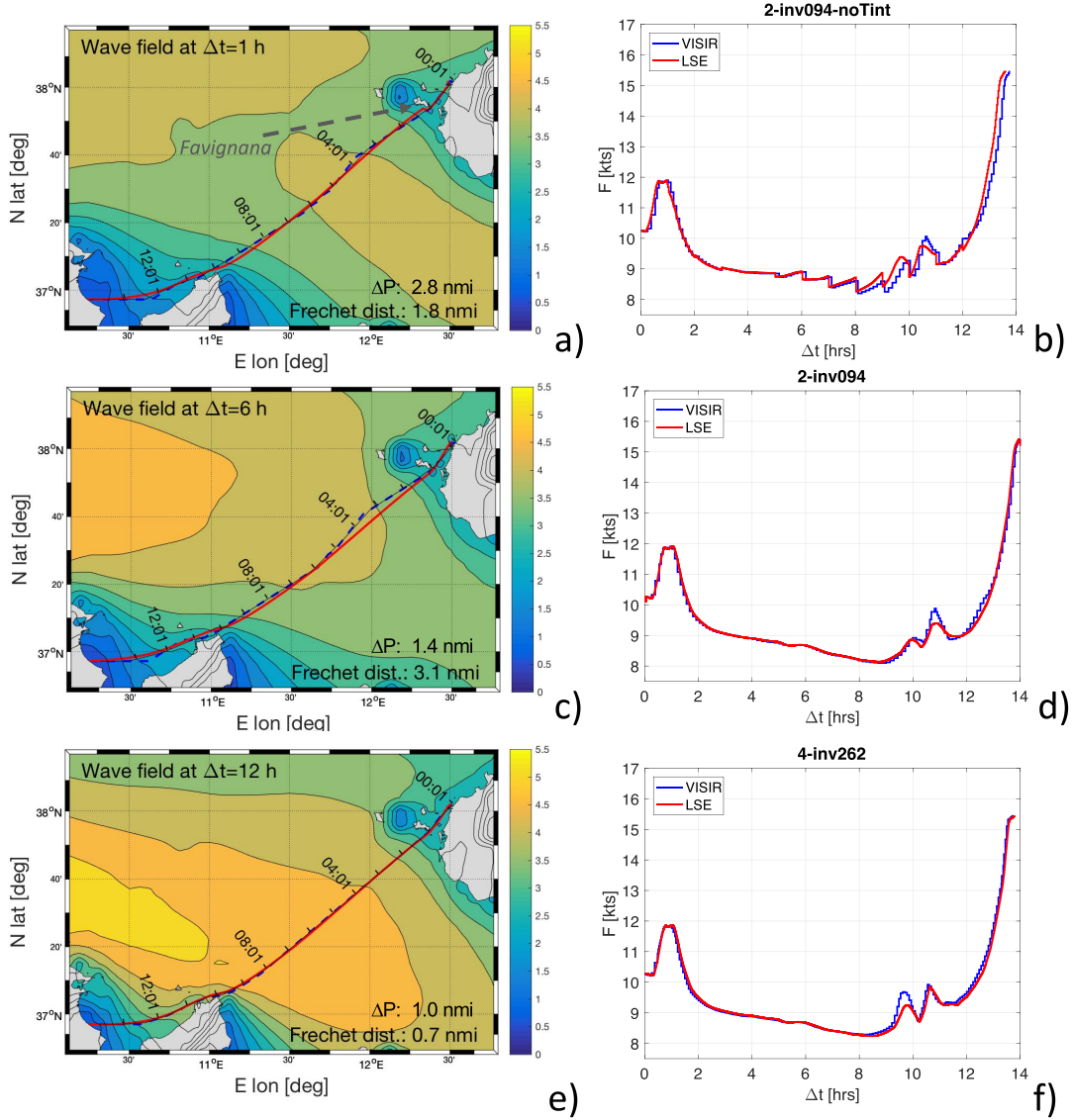7

Fig. 4. Comparison of the VISIR (blue) vs. LSE (red) path maps (left column) and speed timeseries (right column). The first-row panels correspond to the case without time-interpolation. VISIR and LSE mesh resolutions are $1/94°$ and $1/90°$ respectively, in both the first and second row panels and $1/262°$y, and $1/240°$y in the third row panels. Animations of the paths on top of the time-dependent significant wave height field can be viewed at https://av.tib.eu/media/35106, https://av.tib.eu/media/35107, https://av.tib.eu/media/35108, respectively.

by numerical solution to (2–3) in LSE. Again, we emphasize that advection by currents is not used in this test case for either VISIR or LSE, i.e. $\mathbf{V} = 0$ in (2–3). In addition, unlike [41], the dynamical safety constraints on vessel intact stability are disabled in VISIR and not present in LSE. They could be implemented in LSE using the technique for path planning in the presence of moving obstacles developed in [51].

We next compare path and speed profiles in Sect. IV-A, and then study the convergence of the solutions as the discretization error is reduced in Sect. IV-B, and finally analyze the computational costs and the scalings with problem size in Sect. IV-C.

A. Paths and Speed Profiles

The optimal paths and corresponding vessel speed profiles are displayed in Fig. 4 for different graphs $G''(\nu, \Delta x)$.

At all spatial resolutions, the wave field pattern induces a southbound diversion of the paths, which is instrumental in avoiding rough seas and thus realizing higher vehicle speeds through water. Thus, the destination is reached after a time T^* quicker than along the rhumb line between A and B.

The first row (panels a and b) displays a situation similar to that already computed in [41] for VISIR: the graph uses the same order of connectivity ($\nu = 2$) and a 50% finer mesh spacing Δx and, for both VISIR and LSE, the time-interpolation is disabled. However, in this case the updated arc pruning procedure described in Sect. III-B prevents, due to the UKC constraint, all paths from sailing north of Favignana island (ca. 37.93°N, 12.31°E). This was not the case in [41], where a northern passage for the least-distance path ("geodetic route") was computed. The optimal path computed by VISIR exhibits three sudden changes of heading at about 2, 4 and 12 hours after departure: these are due to the

This article has been accepted for inclusion in a future issue of this journal. Content is final as presented, with the exception of pagination.

8

IEEE TRANSACTIONS ON INTELLIGENT TRANSPORTATION SYSTEMS

TABLE II

SUMMARY OF VISIR-LSE COMPARISON METRICS FOR THE PRESENT CASE STUDY (DYNAMIC WAVES BUT ADVECTION-FREE). N_t, n_g, A ARE THE NUMBERS OF TIME STEPS, MESH GRID POINTS, AND GRAPH ARCS, RESPECTIVELY

model	$1/\Delta x$	ν	T-interp	N_t	n_g	A	CPU time opt [s]	CPU time tot [s]	$T^*(\mathbf{x}_B; \mathbf{x}_A)$ [hrs]	$L(\mathbf{x}_B; \mathbf{x}_A)$ [nmi]
	30.0	1	y	16	3 724	28 688	1.3	4.8	14.5911	140.35
	47.4	2	y	16	9 305	214 908	9.1	15.1	13.9558	130.89
VISIR	67.1	3	y	16	18 642	861 430	35.2	48.7	13.7894	130.53
($\Delta P = 2.8$ nmi)	87.5	4	y	16	31 985	2 465 004	102.0	135.0	13.7424	129.99
	108.2	5	y	16	48 920	5 657 446	228.2	301.0	13.7206	130.16
	129.0	6	y	16	69 623	11 275 440	458.8	586.8	13.7301	130.93
	150.0	7	y	16	93 954	20 294 288	829.7	1082.6	13.7278	130.93
	60.0	1	y	16	14 993	117 642	5.8	12.7	14.6275	140.42
	94.9	2	n	16	37 564	883 882	9.7	43.3	13.7742	131.52
VISIR	94.9	2	y	16	37 564	883 882	42.4	75.7	14.0340	132.10
($\Delta P = 1.4$ nmi)	134.2	3	y	16	75 023	3 531 744	160.8	232.8	13.7939	130.59
	174.9	4	y	16	127 882	10 036 000	461.8	651.1	13.7420	130.19
	216.3	5	y	16	195 870	23 061 464	1041.1	1529.3	13.7356	130.71
	90.0	1	y	16	33 774	266 716	15.6	30.5	14.6607	140.52
VISIR	142.3	2	y	16	84 443	1 999 666	109.2	176.6	13.8992	131.02
($\Delta P = 1.0$ nmi)	201.3	3	y	16	168 937	8 003 026	441.7	668.9	13.7707	131.18
	262.4	4	y	16	288 415	22 775 600	1225.1	1866.7	13.7356	130.69
	60.0	-	y	1 415	14 993	-	3.9	21.3	14.15	128.74
	90.0	-	n	510	33 916	-	3.2	17.4	13.60	129.72
LSE	90.0	-	y	1 400	33 916	-	8.8	47.9	14.00	128.97
	120.0	-	y	1 395	60 447	-	15.6	85.2	13.95	129.10
	240.0	-	y	1 379	241 415	-	62.4	340.8	13.79	129.84

coarse angular resolution of the graph. Instead, at this Δx, the LSE path is smoother than that of VISIR. The speed profiles of both VISIR and LSE (Fig. 4b) show, starting from about 5 hours since departure, the saw-tooth feature that was already noted in [41] and which is due to the onset of the hourly time steps of the significant wave height field.

The second row (panels c,d) displays the results on the same VISIR graph and LSE mesh of (panels a,b) upon application of time-interpolation, cf. Sect. III-C. Even though in this case the topological part of the optimal paths is not significantly modified, the speed profiles are altered. They are now much smoother for both VISIR and LSE and do not contain any saw-tooth feature. This leads to navigation time savings of about 20 minutes, cf. Tab. II.

The third row (panels e and f) displays the results at the best spatial and angular resolution, using also time interpolation. Both VISIR and LSE path results are smoother. Minor differences are found only in the coastal zone off Tunisia, due to the VISIR path sailing slightly more inshore, where a better sea state and thus a higher vessel speed are experienced. At even higher resolution, these differences should disappear and the VISIR time-optimal path then converges with that of the LSE.

The three path comparisons are also analyzed in terms of the Fréchet distance between the VISIR and the LSE solution [65]. The values reported in Fig. 4a.c.e are found to be in the order of path resolution ΔP (cf. Tab. II) or smaller.

B. Convergence of Solution Metrics

Two metrics are considered for evaluating the impact of discretization errors: the optimal voyage duration $T^*(\mathbf{x}_B, \mathbf{x}_A)$, which is the objective of the optimization, and the corresponding length $L(\mathbf{x}_B; \mathbf{x}_A)$ of the optimal path. These are displayed in the two panels of Fig. 5.

The various series displayed correspond to different values of the path resolutions ΔP (cf. Sect. III-A). The general trend observed for both T^* and L is that for both VISIR and LSE they converge, increasing mesh parameter $1/\Delta x$.

However, as noted in Sect. III-A, for T^* from a graph-search method to converge it is necessary to increase both mesh and angular resolution. If only the mesh resolution is changed, no new headings are available and the path cannot be made spatially (L) shorter as the mesh resolution is increased. For example, at $\nu = 1$ only headings $\hat{h} \in \{$N, NE, E, SE, S, SW, W, NW$\}$ directions are possible. This results in the length L of VISIR optimal paths being nearly independent of Δx for $\nu = 1$, Fig. 5b. For larger ν values, the variability of L with Δx is limited to the order of magnitude of the mesh spacing.

For VISIR, both T^* and L plots exhibit oscillations, which are more pronounced for the L datapoints, Fig. 5. These probably result from the existence of a common set of arcs in the graphs of identical ΔP but different $(\nu, \Delta x)$. This enables the optimal path to have a similar length on the two different graphs. Due to the spatial inhomogeneity of the wave field, the same L may still lead to different T^*, and thus T^* oscillations are less pronounced.

This article has been accepted for inclusion in a future issue of this journal. Content is final as presented, with the exception of pagination.

MANNARINI *et al.*: GRAPH-SEARCH AND DIFFERENTIAL EQUATIONS FOR TIME-OPTIMAL VESSEL ROUTE PLANNING 9

Fig. 6. Optimal route CPU times as a function of grid spacing n_g. Least-square fits of power-law trends (lines) are also displayed. VISIR and LSE results are portrayed as blue and red symbols, respectively. $\Delta P = [2.8, 1.4, 1.0]$ nmi, respectively, for the low (l), medium (m) and high (h) resolution series.
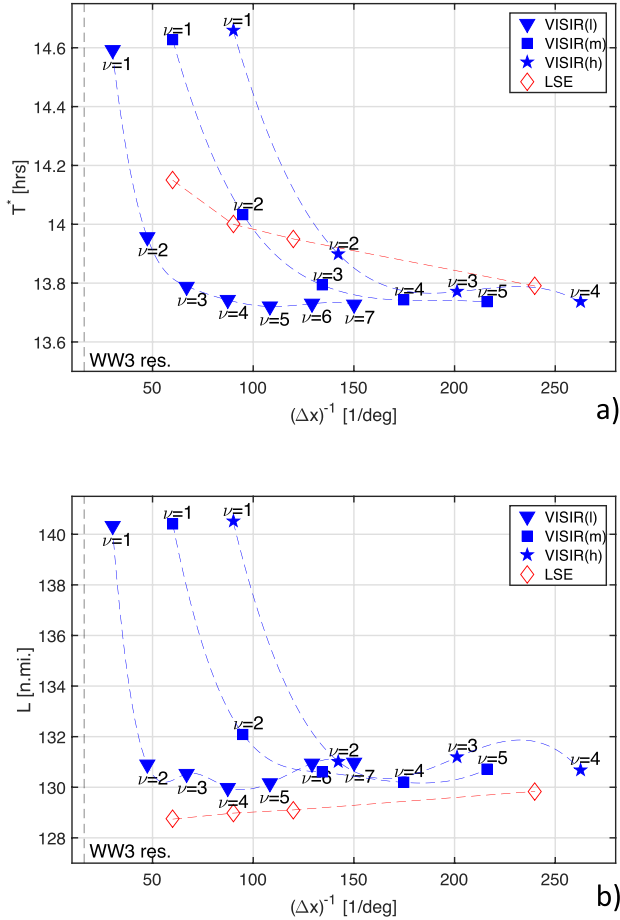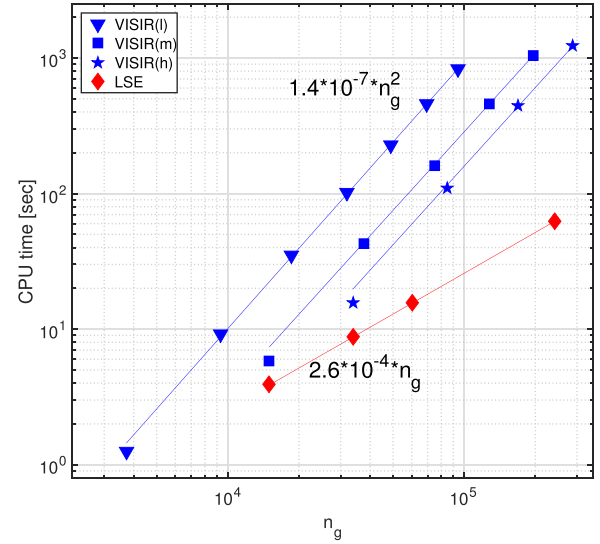

Fig. 5. Optimal path durations $T^*(\mathbf{x}_B; \mathbf{x}_A)$ (panel a) and corresponding path lengths $L(\mathbf{x}_B; \mathbf{x}_A)$ (panel b) as functions of mesh parameter $1/\Delta x$: VISIR datapoints (blue filled symbols) are also labelled by the order of connectivity ν. For a given ΔP they are joined by a spline interpolation (solid blue lines). $\Delta P = [2.8, 1.4, 1.0]$ nmi, respectively, for the low (l), medium (m) and high (h) resolution series. LSE datapoints are displayed as empty red diamonds. The mesh spacing $(1/16°)$ of the WW3 wave model fields used in the input is marked by a dashed vertical line.

This behaviour in the graph-search method of VISIR contrasts with the exact time-differential method of LSE, where convergence of T^* is achieved by only increasing mesh resolution Δx. In fact, in LSE new headings are generated by projecting normals to the reachability front, cf. first term on the r.h.s. of (3). This leads to a T^* that monotonously converges to about 13.8 hours, with a negative slope. For the lengths, LSE convergence to the asymptotic value $L = 130$ nmi instead occurs with a positive slope because, as for the coarser meshes, the path endpoints are closer. Those too inshore cannot be chosen because of the initialization of the reachability front of the LSE method (to reach the coastline a direct travel-time model is commonly used, which is in agreement with real ship practices in the vicinity of harbours). Thus, for too coarse meshes, LSE underestimates L and, in turn, T^*. VISIR endpoints can instead be placed exactly at the coastline, at any graph mesh resolution.

Finally, Fig. 5 shows that to achieve the convergence of the solution, meshes of quite high spatial resolutions must be used. In particular, Δx must be decreased by at least one order of magnitude with respect to the resolution of the wave fields

provided as inputs to both VISIR and LSE. This is as expected for the hyperbolic PDE (2).

C. Scaling of the Computational Cost

For completing the assessment of VISIR with respect to the exact time-differential method of LSE, we next compare the computational costs of their solutions. First, we note that:

i) Similar computers were used: VISIR results were computed on a 3.5GHz, Intel Core i7, 32 GB RAM, DDR3 iMac and those for LSE on a 3GHz, quad core, 16 GB RAM, DDR2 PC (the evaluation experiment was carried out at two different Institutions);

ii) The VISIR total computational time reported here does not include the time for graph computation and pre-processing (cf. Sect. III-B).

iii) LSE data consists of empirical data for the lowest resolution case ($\Delta x = 1/60^o$) and nominal data for all other cases.

All performance data is reported in Tab. II, together with the parameters characterizing the size of the numerical problems. The CPU times for the computation of the optimal routes are displayed as functions of the number n_g of spatial gridpoints in Fig. 6. While LSE is linear in n_g [25], VISIR currently scales as n_g^2 (as expected from a basic implementation of Dijkstra's algorithm [46]).

The scaling laws are not affected by the different hardware used for the numerical tests. The main aim of the present evaluation exercise was to evaluate and validate the previously published solution of VISIR, in which the Dijkstra's algorithm did not include binary heaps or a priority queue. In the future, more advanced performance experiment can be completed when the VISIR shortest path algorithm uses data structures enabling ideal scaling $\mathcal{O}(n_g \log n_g)$. We note that such data structures would be invasive in the VISIR code validated through the present exercise, without changing its

This article has been accepted for inclusion in a future issue of this journal. Content is final as presented, with the exception of pagination.

10

IEEE TRANSACTIONS ON INTELLIGENT TRANSPORTATION SYSTEMS

TABLE III
SUMMARY OF VISIR AND LSE COMPUTATIONAL PERFORMANCE AND
GOODNESS-OF-FIT. THE FIT FUNCTION IS $a \cdot (n_g)^b$

model	type	ΔP [nmi]	a [s]	b [−]	rmse [s]
VISIR	optimal route	2.8	1.36e-07	1.97	1.42
	total job		1.69e-07	1.97	6.54
	optimal route	1.4	6.75e-08	1.93	2.98
	total job		5.70e-08	1.97	11.02
	optimal route	1.0	3.71e-08	1.93	5.88
	total job		6.21e-08	1.92	0.09
LSE	optimal route	-	2.58e-04	1.00	0.02
	total job		1.41e-03	1.00	0.14

solution (optimal path and duration). This contrasts with the modifications made here for the time-interpolation of edge weights Sect. III-C, which also affected and improved the VISIR solution.

For both VISIR and LSE, the actual number of Degrees of Freedom per time step (DOF) and its dependence on grid spacing Δx can be estimated as follows. First, we note that in a rectangular mesh there are $n_g \sim (1/\Delta x)^2$ gridpoints.

Then, for VISIR, the shortest path algorithm depends on the number A of arcs, scaling as $\mathcal{D}_\nu n_g$, cf. (4). In a graph conserving path resolution, the ν parameter varies with $(1/\Delta x)$, cf. (6). This finally results in:

$$DOF_{\text{VISIR}} = A = \mathcal{O}(\nu^2 n_g) \sim (1/\Delta x)^4 \qquad (10)$$

For LSE, the DOF is only given by the number of grid points n_g:

$$DOF_{\text{LSE}} = n_g = \mathcal{O}(n_g) \sim (1/\Delta x)^2 \qquad (11)$$

Thus, mesh refinement is computationally more expensive in VISIR, as the graph connectivity has to be increased to preserve the path resolution (cf. ΔP in Fig. 3). If the path resolution is not preserved, convergence of the solution (cf. datapoints of given ν in Fig. 5) cannot be achieved in a graph-search method.

V. CONCLUSION

In this study, an initial evaluation of a graph-search approach for time-optimal path planning in dynamic ocean surface gravity waves (VISIR) was completed by comparing it with a numerical solver of the governing differential equations for such path planning (LSE). The comparison also allows for the validation of VISIR's optimal path planning in time-dependent wave fields, which commonly constrain the cruising speed of ships.

VISIR and LSE were compared to compute time-optimal paths without advection by ocean currents. Under these conditions (ocean current speed is null, thus less than vessel speed), the graph-search method also solves the exact time-optimal path.

After several technical improvements (the time-interpolation and masking procedure in VISIR, and vessel speed loss in waves for LSE, Sect. III), we indeed found that the VISIR solution became similar to and converged to that of LSE.

As shown in Sect. IV, the two approaches obviously differ in their key ideas, numerical implementation, performance, and capabilities to manage limit conditions (e.g. currents stronger than vessel velocity, delayed start of the path, and non-FIFO arc weights for LSE; and in direct coastal endpoints for VISIR). We note that for VISIR (and a graph-search method in general) to converge, it is not sufficient to simply increase the mesh resolution. The new procedure for mesh refinement and contextual increase in graph connectivity (Sect. III-A and Fig. 3) is necessary, cf. (6).

To complement the analysis, a preliminary assessment of the computational performance of the two numerical solvers in their present implementation was provided. The present VISIR code performance scales such as n_g^2 and could be improved at most to $n_g \log n_g$. The LSE cost scales linearly with the number of grid points n_g. Thus, the present LSE software delivered the results on the finest mesh in about 5 minutes, while the corresponding VISIR results were obtained in about a 5 times that duration.

The capability to deal with advection by ocean currents has also recently been introduced in VISIR for vessels faster than the flow [43]. Instead, for small or very slow surface vessels, the computational cost of the graph search method may significantly increase. It could even lead to suboptimal solutions if the magnitude of local currents exceeds the top vessel speed (local controllability). In [66] a graph based method was tested versus an optimal control method for AUV path planning, requiring an adaptive time step for delivering the correct results. In future, this needs to be investigated also through VISIR.

Nevertheless, the present paper provides, to our knowledge, the first quantitative comparison and convergence analysis of two end-to-end path planning systems for a realistic ship routing application.

Additional areas of development for VISIR may include some problems already addressed through the LSE, such as interceptions and multi-waypoint missions [29], [55], [56], energy optimization [54], onboard learning [57], and clustering of vessels to low-risk routes in uncertain flow environments [67]–[69].

APPENDIX A
VESSEL INTERACTION WITH WAVES

Maritime path planning is particular to the terrestrial routing and the specific vessel type can make a difference. The VISIR model version assessed by the present evaluation exercise refers to some of the vessel types sailing in the Mediterranean Sea (fishing vessels, short trip coastal freighters, displacement hull, yachts and pleasure crafts, and small ferry boats). In the present exercise a ferry boat is considered, and the speed loss in waves (cf. Sect. III) corresponds to the parameterization documented in detail in [41], and is briefly reviewed as follows.

The propulsion system delivers, through the main engine, shaft and eventually the gearbox, a power P_p to the propeller. In the steady state, P_p balances the power dissipated by the resistance acting on the propeller. The latter consists of a calm

This article has been accepted for inclusion in a future issue of this journal. Content is final as presented, with the exception of pagination.

MANNARINI *et al.*: GRAPH-SEARCH AND DIFFERENTIAL EQUATIONS FOR TIME-OPTIMAL VESSEL ROUTE PLANNING 11

water R_c and a wave-added component R_{aw}. R_c includes the frictional and wave making resistance and is parametrized as a polynomial in vessel STW. R_{aw} is a parametrization of pitch and heave energy loss, based on a statistical reanalysis of numerical simulations via Gerritsma and Beukelman's method [70]. It depends only on vessel length, beam, draught, and significant wave height. The vessel top-speed allows for the value of the wetted surface to be identified, which is given in R_c. The power balance results in the vessel speed being one of the roots of a polynomial equation.

The relation of this vessel model to typical issues in navigation is briefly reviewed as follows:

- **Currents** are addressed by the new VISIR model version [43], accounting for vector composition of ocean velocity and vessel STW;
- **Winds** are not yet dealt with in the VISIR modelling of motorboats, and only sailboat routing though a polar diagram is considered [44]. This has also been implemented in LSE. The effect of wind is important for vessels with a large superstructure and will be considered in VISIR in a new project[5];
- **Fuel consumption** is proportional to engine break power P_p and sailing time T^*. In [43], and optimal path computations are performed to account for both factors;
- **Emissions** in [43] the impact of VISIR path optimization on CO_2 emissions was assessed through the use of an indicator of carbon intensity (EEOI) defined by the International Maritime Organization.
- **Safety** constraints for intact stability are included in VISIR. However, they were not considered for the present evaluation as the focus of the manuscript was an assessment of VISIR as a path planner. Dynamic safety constraints can also be addressed in LSE by means of masking [51];
- **Manoeuvrability** issues may arise from too rapid changes in either vessel heading $\hat{h}$ and/or engine power setting P_p. Vessel turn radius [71] typically reads a few vessel length units, which is less than 1 nmi for the vessel under consideration. $\hat{h}$ changes in Fig. 4 imply a radius of curvature of several tens of miles, which is large enough with respect to the vessel rate of turn. P_p is kept constant within both VISIR and LSE for the sake of this exercise. For open-sea navigation, which is well outside the zone where ship acceleration/deceleration transients usually occur, this is an acceptable approximation.

A recent evaluation of time-optimal trajectories computed by VISIR and actually sailed trajectories in the Southern Atlantic Ocean was conducted in [72]. These preliminary results indicate that only part of the actually sailed trajectories are to some extent optimized.

APPENDIX B
PSEUDOCODE OF THE VISIR TIME-DEPENDENT ALGORITHM

In the following pseudocode, j_s, j_e are the start and end path node, respectively; f_k is the predecessor ("father") of node k

[5]http://www.bit.ly/guttaproject

Algorithm 1 DIJKSTRA_TIME-INTERP

1 inputs: j_s, j_e, $\{(jk)\}$, $\{a_{jk\ell}\}$
2 *Initialization:*
3 $\quad \tau_s \leftarrow t_1, f_s \leftarrow$ NaN
4 $\quad \forall k \neq s \quad \sigma_k \leftarrow \infty, \tau_k \leftarrow 0, f_k \leftarrow$ NaN
5 $\quad j \leftarrow j_s$
6 **if** *T-interp* **then**
7 $\quad\big|\quad \mathcal{L} \leftarrow 1 + \tau_j/\Delta_{tE}$
8 **else**
9 $\quad\big|\quad \ell \leftarrow 1 + \text{floor}(\tau_j/\Delta_{tE})$
10 **end if**
11 *Main iteration – part I:*
12 **for** *all neighbours k of j for which $\tau_k = 0$* **do**
13 $\quad\big|\quad$ **if** *T-interp* **then**
14 $\quad\big|\quad\big|\quad b_{jk} = a_{jk}(t)$ linearly interp. at $t = \mathcal{L}$
15 $\quad\big|\quad$ **else**
16 $\quad\big|\quad\big|\quad b_{jk} = a_{jk\ell}$
17 $\quad\big|\quad$ **end if**
18 $\quad\big|\quad \sigma_k \leftarrow \min\{\sigma_k, \tau_j + b_{jk}\}$
19 $\quad\big|\quad$ **if** σ_k changed at line 18, **then set** $f_k \leftarrow j$
20 **end for**
21 *Exit condition:*
22 **if** *j_e has non-null τ value* **then**
23 $\quad\big|\quad$ exit
24 **else**
25 $\quad\big|\quad$ *Main iteration – part II:*
26 $\quad\big|\quad$ find a node l: $\sigma_l = \min\limits_{k \in V} \sigma_k$, $V = \{k : \tau_k = 0\}$
27 $\quad\big|\quad$ set $\tau_l \leftarrow \sigma_l, j \leftarrow l$
28 $\quad\big|\quad$ proceed with *Main iteration – part I*
29 **end if**

---

on the path; NaN is a missing value; (jk) is the oriented arc between j and k node; $a_{jk\ell}$ and $a_{jk}(t)$ are corresponding edge weights at time step ℓ and at time t; σ_k and τ_k are the temporary and permanent labels of node k, respectively.

REFERENCES

[1] K. Boriboonsomsin, M. J. Barth, W. Zhu, and A. Vu, "Eco-routing navigation system based on multisource historical and real-time traffic information," *IEEE Trans. Intell. Transp. Syst.*, vol. 13, no. 4, pp. 1694–1704, Dec. 2012.
[2] K. L. Moore, Y. Chen, and Z. Song, "Diffusion-based path planning in mobile actuator-sensor networks (MAS-Net): Some preliminary results," *Proc. SPIE*, vol. 5421, pp. 58–69, Apr. 2004.
[3] P. F. J. Lermusiaux *et al.*, "Science of autonomy: Time-optimal path planning and adaptive sampling for swarms of ocean vehicles," in *Springer Handbook of Ocean Engineering: Autonomous Ocean Vehicles, Subsystems and Control*, T. Curtin, Ed. Springer, 2016, ch. 21, pp. 481–498.
[4] J. Carsten, A. Rankin, D. Ferguson, and A. Stentz, "Global path planning on board the Mars exploration rovers," in *Proc. IEEE Aerosp. Conf.*, Mar. 2007, pp. 1–11.
[5] V. Grewe *et al.*, "Aircraft routing with minimal climate impact: The REACT4C climate cost function modelling approach (V1.0)," *Geosci. Model Develop.*, vol. 7, no. 1, pp. 175–201, 2014. [Online]. Available: https://www.geosci-model-dev.net/7/175/2014/
[6] M. Christiansen, K. Fagerholt, B. Nygreen, and D. Ronen, "Ship routing and scheduling in the new millennium," *Eur. J. Oper. Res.*, vol. 228, no. 3, pp. 467–483, 2013.
[7] *Third IMO GHG Study 2014*, document MEPC 67/INF.3, International Maritime Organization, London, U.K., 2014.

[8] R. Zoppoli, "Minimum-time routing as an N-stage decision process," *J. Appl. Meteorol.*, vol. 11, no. 3, pp. 429–435, 1972.

[9] H. H. Chen, "A dynamic program for minimum cost ship routing under uncertainty," Ph.D. dissertation, Dept. Ocean Eng., Massachusetts Inst. Technol., Cambridge, MA, USA, 1978.

[10] B. Garau, M. Bonet, A. Alvarez, and S. Ruiz, "Path planning for autonomous underwater vehicles in realistic oceanic current fields: Application to gliders in the Western Mediterranean Sea," *J. Maritime Res.*, vol. 6, no. 2, pp. 5–22, 2009.

[11] D. Rao and S. B. Williams, "Large-scale path planning for underwater gliders in ocean currents," in *Proc. Australas. Conf. Robot. Automat. (ACRA)*, 2009, pp. 1–8.

[12] T. Inanc, S. C. Shadden, and J. E. Marsden, "Optimal trajectory generation in ocean flows," in *Proc. Amer. Control Conf.*, Jun. 2005, pp. 674–679.

[13] D. Kruger, R. Stolkin, A. Blum, and J. Briganti, "Optimal AUV path planning for extended missions in complex, fast-flowing estuarine environments," in *Proc. IEEE Int. Conf. Robot. Autom.*, Apr. 2007, pp. 4265–4270.

[14] W. Zhang, T. Inanc, S. Ober-Blobaum, and J. E. Marsden, "Optimal trajectory generation for a glider in time-varying 2D ocean flows B-spline model," in *Proc. IEEE Int. Conf. Robot. Automat.*, May 2008, pp. 1083–1088.

[15] D. Jones and G. A. Hollinger, "Planning energy-efficient trajectories in strong disturbances," *IEEE Robot. Autom. Lett.*, vol. 2, no. 4, pp. 2080–2087, Oct. 2017.

[16] A. Alvarez, A. Caiti, and R. Onken, "Evolutionary path planning for autonomous underwater vehicles in a variable ocean," *IEEE J. Ocean. Eng.*, vol. 29, no. 2, pp. 418–429, Apr. 2004.

[17] M. P. Aghababa, "Finite-time chaos control and synchronization of fractional-order nonautonomous chaotic (hyperchaotic) systems using fractional nonsingular terminal sliding mode technique," *Nonlinear Dyn.*, vol. 69, nos. 1–2, pp. 247–261, 2012.

[18] J. Witt and M. Dunbabin, "Go with the flow: Optimal AUV path planning in coastal environments," in *Proc. Austral. Conf. Robot. Automat.*, 2008, pp. 1–9.

[19] E. Bakolas and P. Tsiotras, "The Zermelo–Voronoi diagram: A dynamic partition problem," *Automatica*, vol. 46, no. 12, pp. 2059–2067, 2010.

[20] J. A. Sethian, "Fast marching methods," *SIAM Rev.*, vol. 41, no. 2, pp. 199–235, Jun. 1999. doi: 10.1137/S0036144598347059.

[21] C. Petres, Y. Pailhas, P. Patron, Y. Petillot, J. Evans, and D. Lane, "Path planning for autonomous underwater vehicles," *IEEE Trans. Robot.*, vol. 23, no. 2, pp. 331–341, Apr. 2007.

[22] M. Soulignac, P. Taillibert, and M. Rueher, "Time-minimal path planning in dynamic current fields," in *Proc. IEEE Int. Conf. Robot. Autom.*, May 2009, pp. 2473–2479.

[23] D. R. Thompson *et al.*, "Spatiotemporal path planning in strong, dynamic, uncertain currents," in *Proc. IEEE Int. Conf. Robot. Automat. (ICRA)*, May 2010, pp. 4778–4783.

[24] T. Lolla, M. P. Ueckermann, K. Yiğit, P. J. Haley, Jr., and P. F. J. Lermusiaux, "Path planning in time dependent flow fields using level set methods," in *Proc. IEEE Int. Conf. Robot. Automat.*, May 2012, pp. 166–173.

[25] T. Lolla, P. F. Lermusiaux, M. P. Ueckermann, and P. J. Haley, Jr., "Time-optimal path planning in dynamic flows using level set equations: Theory and schemes," *Ocean Dyn.*, vol. 64, no. 10, pp. 1373–1397, Oct. 2014.

[26] T. Lolla, P. J. Haley, Jr., and P. F. J. Lermusiaux, "Time-optimal path planning in dynamic flows using level set equations: Realistic applications," *Ocean Dyn.*, vol. 64, no. 10, pp. 1399–1417, 2014.

[27] P. F. J. Lermusiaux *et al.*, "A future for intelligent autonomous ocean observing systems," *J. Marine Res.*, vol. 75, no. 6, pp. 765–813, Nov. 2017.

[28] D. N. Subramani *et al.*, "Time-optimal path planning: Real-time sea exercises," in *Proc. OCEANS MTS/IEEE Conf.*, Aberdeen, U.K., Jun. 2017, pp. 1–10.

[29] D. L. Ferris, D. N. Subramani, C. S. Kulkarni, P. J. Haley, Jr., and P. F. J. Lermusiaux, "Time-optimal multi-waypoint mission planning in dynamic environments," in *Proc. OCEANS MTS/IEEE Charleston*, Charleston, SC, USA, Oct. 2018, pp. 1–8.

[30] P. C. Chen and Y. K. Hwang, "SANDROS: A dynamic graph search algorithm for motion planning," *IEEE Trans. Robot. Automat.*, vol. 14, no. 3, pp. 390–403, Jun. 1998.

[31] I. Mani and E. Bloedorn, "Multi-document summarization by graph search and matching," 1997, *arXiv:cmp-lg/9712004*. [Online]. Available: https://arxiv.org/abs/cmp-lg/9712004

[32] S.-C. Oh, B.-W. On, E. J. Larson, and D. Lee, "BF: Web services discovery and composition as graph search problem," in *Proc. IEEE Int. Conf. e-Technol., e-Commerce e-Service*, Mar./Apr. 2005, pp. 784–786.

[33] S. E. Dreyfus, "An appraisal of some shortest-path algorithms," *Oper. Res.*, vol. 17, no. 3, pp. 395–412, 1969.

[34] A. Orda and R. Rom, "Shortest-path and minimum-delay algorithms in networks with time-dependent edge-length," *J. ACM*, vol. 37, no. 3, pp. 607–625, 1990.

[35] L. Foschini, J. Hershberger, and S. Suri, "On the complexity of time-dependent shortest paths," *Algorithmica*, vol. 68, no. 4, pp. 1075–1097, 2014.

[36] J. N. Tsitsiklis, "Efficient algorithms for globally optimal trajectories," *IEEE Trans. Autom. Control*, vol. 40, no. 9, pp. 1528–1538, Sep. 1995.

[37] P. E. Hart, N. J. Nilsson, and B. Raphael, "A formal basis for the heuristic determination of minimum cost paths," *IEEE Trans. Syst. Sci. Cybern.*, vol. SSC-4, no. 2, pp. 100–107, Jan. 1968.

[38] A. Stentz and I. C. Mellon, "Optimal and efficient path planning for unknown and dynamic environments," *Int. J. Robot. Automat.*, vol. 10, pp. 89–100, Aug. 1993.

[39] S. M. Lavalle, "Rapidly-exploring random trees: A new tool for path planning," Iowa State Univ., Ames, IA, USA, Tech. Rep. TR 98-11, 1998.

[40] C. Pêtrès, M.-A. Romero-Ramirez, and F. Plumet, "A potential field approach for reactive navigation of autonomous sailboats," *Robot. Auton. Syst.*, vol. 60, no. 12, pp. 1520–1527, 2012.

[41] G. Mannarini, N. Pinardi, G. Coppini, P. Oddo, and A. Iafrati, "VISIR-I: Small vessels—Least-time nautical routes using wave forecasts," *Geosci. Model Develop.*, vol. 9, no. 4, pp. 1597–1625, 2016. [Online]. Available: http://www.geosci-model-dev.net/9/1597/2016/

[42] G. Mannarini *et al.*, "VISIR: Technological infrastructure of an operational service for safe and efficient navigation in the Mediterranean Sea," *Natural Hazards Earth Syst. Sci.*, vol. 16, no. 8, pp. 1791–1806, 2016. [Online]. Available: http://www.nat-hazards-earth-syst-sci.net/16/1791/2016/

[43] G. Mannarini and L. Carelli, "VISIR-1.b: Ocean surface gravity waves and currents for energy-efficient navigation," *Geosci. Model Develop.*, vol. 12, no. 8, pp. 3449–3480, 2019. [Online]. Available: https://www.geosci-model-dev.net/12/3449/2019/

[44] G. Mannarini, R. Lecci, and G. Coppini, "Introducing sailboats into ship routing system VISIR," in *Proc. 6th Int. Conf. Inf., Intell., Syst. Appl. (IISA)*, Jul. 2015, pp. 1–6.

[45] E. W. Dijkstra, "A note on two problems in connexion with graphs," *Numer. Math.*, vol. 1, no. 1, pp. 269–271, Dec. 1959.

[46] D. P. Bertsekas, *Network Optimization: Continuous and Discrete Models*. Belmont, MA, USA: Athena Scientific, 1998.

[47] R. K. Ahuja, T. L. Magnanti, and J. B. Orlin, "Network flows," Massachusetts Inst. Technol., Cambridge, MA, USA, Sloan W.P. No. 2059-88, 1988.

[48] E. Clementi, P. Oddo, M. Drudi, N. Pinardi, G. Korres, and A. Grandi, "Coupling hydrodynamic and wave models: First step and sensitivity experiments in the mediterranean sea," *Ocean Dyn.*, vol. 67, no. 10, pp. 1293–1312, 2017. doi: 10.1007/s10236-017-1087-7.

[49] W. H. Press, S. A. Teukolsky, W. T. Vetterling, and B. P. Flannery, *Numerical Recipes in C*, vol. 2. Cambridge, U.K.: Cambridge Univ. Press, 1996.

[50] P. Pérez, M. Gangnet, and A. Blake, "Poisson image editing," in *Proc. ACM SIGGRAPH Papers*, New York, NY, USA, 2003, pp. 313–318. [Online]. Available: http://doi.acm.org/10.1145/1201775.882269

[51] T. Lolla, P. J. Haley, Jr., and P. F. J. Lermusiaux, "Path planning in multi-scale ocean flows: Coordination and dynamic obstacles," *Ocean Model.*, vol. 94, pp. 46–66, Oct. 2015.

[52] D. N. Subramani, T. Lolla, P. J. Haley, Jr., and P. F. J. Lermusiaux, "A stochastic optimization method for energy-based path planning," in *Proc. DyDESS*, in Lecture Notes in Computer Science, vol. 8964, S. Ravela and A. Sandu, Eds. Cham, Switzerland: Springer, 2015, pp. 347–358.

[53] D. N. Subramani and P. F. J. Lermusiaux, "Energy-optimal path planning by stochastic dynamically orthogonal level-set optimization," *Ocean Model.*, vol. 100, pp. 57–77, Apr. 2016.

[54] D. N. Subramani, P. J. Haley, Jr., and P. F. J. Lermusiaux, "Energy-optimal path planning in the coastal ocean," *J. Geophys. Res., Oceans*, vol. 122, no. 5, pp. 3981–4003, 2017.

[55] C. Mirabito *et al.*, "Autonomy for surface ship interception," in *Proc. OCEANS MTS/IEEE Conf.*, Aberdeen, U.K., Jun. 2017, pp. 1–10.

This article has been accepted for inclusion in a future issue of this journal. Content is final as presented, with the exception of pagination.

MANNARINI *et al.*: GRAPH-SEARCH AND DIFFERENTIAL EQUATIONS FOR TIME-OPTIMAL VESSEL ROUTE PLANNING 13

[56] W. Sun, P. Tsiotras, T. Lolla, D. N. Subramani, and P. F. J. Lermusiaux, "Multiple-pursuer/one-evader pursuit–evasion game in dynamic flow-fields," *J. Guid., Control, Dyn.*, vol. 40, no. 7, pp. 1627–1637, Apr. 2017.

[57] J. Edwards *et al.*, "Data-driven learning and modeling of AUV operational characteristics for optimal path planning," in *Proc. OCEANS MTS/IEEE Conf.*, Aberdeen, U.K., Jun. 2017, pp. 1–5.

[58] J. H. Ferziger and M. Peric, *Computational Methods for Fluid Dynamics*. Berlin, Germany: Springer-Verlag, 2012.

[59] J. A. Sethian, *Level Set Methods and Fast Marching Methods: Evolving Interfaces in Computational Geometry, Fluid Mechanics, Computer Vision, and Materials Science*, vol. 3. Cambridge, U.K.: Cambridge Univ. Press, 1999.

[60] R. Diestel, *Graph Theory*. Heidelberg, Germany: Springer-Verlag, 2010. [Online]. Available: http://diestel-graph-theory.com/

[61] M. Grifoll and F. M. de Osés, "A ship routing system applied at short sea distances," *J. Maritime Res.*, vol. 13, no. 2, pp. 3–6, 2016.

[62] J. C. H. Cheung, "Flight planning: Node-based trajectory prediction and turbulence avoidance," *Meteorolog. Appl.*, vol. 25, no. 1, pp. 78–85, 2017.

[63] A. Veneti, A. Makrygiorgos, C. Konstantopoulos, G. Pantziou, and I. A. Vetsikas, "Minimizing the fuel consumption and the risk in maritime transportation: A bi-objective weather routing approach," *Comput. Oper. Res.*, vol. 88, pp. 220–236, Dec. 2017.

[64] N. Pinardi *et al.*, "Mediterranean Sea large-scale low-frequency ocean variability and water mass formation rates from 1987 to 2007: A retrospective analysis," *Prog. Oceanogr.*, vol. 132, pp. 318–332, Mar. 2015.

[65] T. Eiter and H. Mannila, "Computing discrete Fréchet distance," Technische Univ. Wien, Wien, Austria, Tech. Rep. CD-TR 94/64, 1994.

[66] D. Kularatne, S. Bhattacharya, and M. A. Hsieh, "Optimal path planning in time-varying flows using adaptive discretization," *IEEE Robot. Autom. Lett.*, vol. 3, no. 1, pp. 458–465, Jan. 2017.

[67] A. Dutt, D. N. Subramani, C. S. Kulkarni, and P. F. J. Lermusiaux, "Clustering of massive ensemble of vehicle trajectories in strong, dynamic and uncertain ocean flows," in *Proc. OCEANS MTS/IEEE Charleston*, Charleston, SC, USA, Oct. 2018, pp. 1–7.

[68] D. N. Subramani, Q. J. Wei, and P. F. J. Lermusiaux, "Stochastic time-optimal path-planning in uncertain, strong, and dynamic flows," *Comput. Methods Appl. Mech. Eng.*, vol. 333, pp. 218–237, May 2018.

[69] D. N. Subramani and P. F. J. Lermusiaux, "Risk-optimal path planning in stochastic dynamic environments," *Comput. Methods Appl. Mech. Eng.*, vol. 353, pp. 391–415, Aug. 2019.

[70] J. Gerritsma and W. Beukelman, "Analysis of the resistance increase in waves of a fast cargo ship," *Int. Shipbuilding Prog.*, vol. 19, no. 217, pp. 285–293, 1972.

[71] *Guide for Vessel Maneuvrability*, Amer. Bureau Shipping, Houston, TX, USA, 2017.

[72] G. Mannarini, L. Carelli, D. Zissis, G. Spiliopoulos, and K. Chatzikokolakis, "Preliminary inter-comparison of AIS data and optimal ship tracks," *TransNav, Int. J. Mar. Navigation Saf. Sea Transp.*, vol. 13, no. 1, pp. 53–61, 2019.

Deepak N. Subramani received the M.Tech. degree in mechanical engineering from IIT Madras, Chennai, in 2012, and the M.Sc. degree in computation for design and optimization and the Ph.D. degree in mechanical engineering and computational engineering from the Massachusetts Institute of Technology, in 2014 and 2017, respectively. During his Ph.D., he developed a probabilistic regional ocean prediction system, optimal vehicle guidance schemes, and advisory services for sustainable fisheries management in India. He is currently an Assistant Professor with the Department of Computational and Data Sciences, Indian Institute of Science (IISC), Bengaluru, India. He focuses on developing fundamental knowledge for usable systems that solve practical problems.

Pierre F. J. Lermusiaux is currently a Professor of mechanical engineering and ocean science and engineering with the Massachusetts Institute of Technology (MIT), Cambridge, USA, and an Associate Department Head of research and operations in mechanical engineering. He received a Fulbright Foundation Fellowship in 1992, the Wallace Prize at Harvard in 1993, the Ogilvie Young Investigator Lecture in Ocean Engineering, MIT, in 1998, and the MIT Doherty Chair in Ocean Utilization from 2009 to 2011. In 2010, the School of Engineering, MIT, where he received the Ruth and Joel Spira Award for Distinguished Teaching. He has made outstanding and fundamental contributions in data assimilation, and in ocean modeling and uncertainty predictions. His research interests include understanding and modeling complex physical and interdisciplinary oceanic dynamics and processes. He has participated in many national and international sea exercises, and has served in numerous committees and organized major meetings.

Gianandrea Mannarini received the M.Sc. degree in physics from the Università degli Studi di Pisa, Italy, in 2000, and the Ph.D. degree in theoretical physics from the Humboldt-Universität zu Berlin, Germany, in 2005. Since 2012, he has developed from scratch the VISIR ship routing model as a downstream application of meteo-ocanographic operational products. He is currently a Scientist with the Centro Euro-Mediterraneo sui Cambiamenti Climatici (CMCC), Lecce, Italy, where he leads the Applications Research Unit of the OPA Division. His research interests include the environmental impact of maritime navigation, particularly in terms of climate change, and the automation of data services. His work on VISIR achieved the Best Presentation Award at the TransNav2019 Conference. He coordinates the GUTTA project on maritime transportation in the Adriatic Sea, which is a part of the Italy–Croatia Interreg Programme.

Nadia Pinardi received the Ph.D. degree in applied physics from Harvard University, USA. She is currently a Full Professor of oceanography with the Università di Bologna, Italy. Since the mid-1990s, she has been coordinating the development and implementation of operational oceanography in the Mediterranean Sea. She has written more than 100 papers in peer-reviewed journals on a wide range of subjects. Her interests range from ocean numerical modeling and forecasting to data assimilation, predictability and numerical modeling of marine physical-biological interactions. In 2007, she received the European Geophysical Union (EGU) Fridtjof Nansen Medal for Oceanography and in June 2008 the Roger Revelle UNESCO Medal. She is the Co-President of the Joint Committee for Oceanography and Marine Meteorology (JCOMM).